Point Spread Function Modelling for the Restoration of 3D Images from The Episcopic Fluorescence Image Capturing System

Daan Zhu*, Timothy Mohun* and Stamatis N. Pagakis**

* National Institute for Medical Research, London, England
** Foundation for Biomedical Research, Academy of Athens, Athens, Greece

dzhu@nimr.mrc.ac.uk

Abstract: Our work aims at the reconstruction of three dimensional (3D) fluorescence microscopy images which are obtained from the Episcopic Fluorescence Image Capturing (EFIC) system. The images are of high resolution and exactly aligned in the z-axis making them ideal for producing volume data sets by virtual stacking of the images. However some of the fluorescence detected in any image of the block surface nevertheless originates from tissue within the wax. To correct this problem, the raw PSF was obtained from the experimental fluorescence microscopy images and a Gradient Descent Algorithm (GDA) was employed to model the Point Spread Function (PSF) of the EFIC. A minimum error between the target function and raw data was approached through an iterative solution. The modelled PSF was then combined with the Landweber deconvolution algorithm in order to restore the 3D data for reconstruction.

Introduction

Episcopic fluorescence imaging is based on capturing successive fluorescence images of the top surface of wax embedded biological specimens during serial sectioning. The images are of high resolution and exactly aligned in the z-axis making them ideal for producing volume data sets by virtually stacking them. The embedded tissue is visualised by virtue of its autofluorescence which varies according to cell or tissue type and provides a detailed view of morphology [1]. In order to ensure that the fluorescence detected at the block surface only results from the tissue at the block surface, dyes are incorporated in the wax embedding medium to supress fluorescence from any portion of the specimen below the surface. Whilst this is reasonably effective, some of the fluorescence detected in any image of the block surface nevertheless originates from tissue within the wax. Figure 1 shows a sample image stack (showing a region of a mouse embryo heart) from the XY (left) and XZ (right) planes. The tailed points in the XZ planes are the bright fluorescent objects which stay visible for many sections along the z direction. This compromises the quality of individual images and the resolution of 3D data sets. Deconvolution technique is an ideal method of restoring the out-of-focus blurr from fluorescence microscopy images. The point spread function (PSF) of an imaging system provides a complete, quantitative description of the imaging process and directly characterizes the image degradation within the system and needs to be known in advance. Measurement of the PSF based on an experimental data set has been developed before. Zhu et.al. and Razaz et.al. modelled the PSF from the raw data in X-ray diffraction [2] and Nuclear Magnetic Resonance (NMR) imaging [3,4]. Quabis [5] summarized experimental and theoretical methods to measure the PSF of microscope tomography.

In this paper a novel algorithm is introduced to model the EFIC PSF. The interfering fluorescence from below the surface can be simplified into a diffusive motion-like blur along the z-direction. The approximation of the raw PSF is collected from the original 3D episcopic fluorescence microscopy images in the form of an isolated spot along the z axis. In the frequency domain, the optical transform function (OTF), which is approximated by a [**sinc(x,y,z)**], is used as a target function. The minimum error between the target function and the approximate PSF is approached by the Gradient Descent Algorithm (GDA). Using this approach, a reliable 3D restoration model is developed to remove the out-of-focus interference from the original image stack.

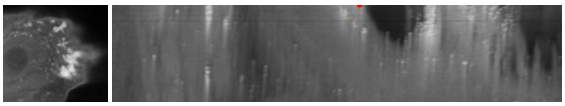

Figure 1. Image slice in the XY and XZ plane

Modelling and Mathematical Methods

The process of deconvolution in an imaging system can be described by the matrix equation $\mathbf{g} = \mathbf{Hf}+\mathbf{n}$ [6], where **H** is a degradation matrix representing the effect of data blurring by the PSF, **f** is a vector representing the source image, **g** is the observed image and **n** is the additive noise [6, 7]. We can see from this equation that the knowledge of PSF is essential for formulating the matrix **H** and hence finding the source image **f**. In many cases **H** is very large and ill-posed making the restoration of **f** a non-trivial task.

Several traditional mathematical formulas have been used to model the PSF such as Gaussian or Bessel functions. Zhu [8] modeled the out-of-focus PSF using a two dimensional (2D) Motiff function. Whichever function is used to model the PSF of a microscopy imaging system, the PSF is always considered to be

ISSN: 1727-1983

circularly symmetric. These types of PSFs can be used to model the out-of-focus effects commonly occurring in optical imaging systems. The modeled PSF is then combined with the deconvolution algorithms such as Maximum Likelihood Expectation Maximization (MLEM), Iterative Deconvolution Algorithm (IDA) [9] to restore blurred microscopy images.

However, the PSF of an episcopic fluorescence imaging system is not symmetric around the focal point. Whereas in traditional microscopy the out-of-focus part of the PSF is on either side of the focal point, here it is on the one side of it (Figure 11). Therefore, the images obtained on the episcopic fluoresence microscope are aberrated along the z-axis with a diffusive, motion-like blurring. Traditional formulas used to model optical PSFs cannot be used in this case and the normal deconvolution algorithms can not be applied. Figure 2 presents a schematic of the biological sample and the imaging process. The biological tissue is fixed in a wax block. The top surface is photographed by the imaging system, a slice is then removed and the top surface is photographed again. The process is repeated through the whole wax block. The digital 3D image of the specimen is created by the rendering of the individual images from the top to the bottom along the z axis. The thickness of each slice is entirely determined by the experimenter and can vary between 1 and 10 μm. The actual fluorescence microscopy image obtained combines the surface image along with a proportion of the fluorescence from the structures underneath. Therefore the captured image is significantly blurred and the effective image resolution is reduced. In addition, the absence of clear edges in the data compromises its use for 3D visualization and reconstruction. These problems are demonstrated in figures 3 and 4 which show experimental image slices along the XY and YZ planes respectively.

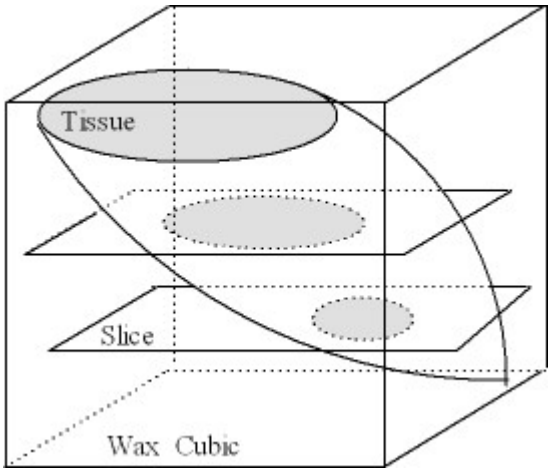

Figure 2. Schematic of a biological tissue embeded in the wax block

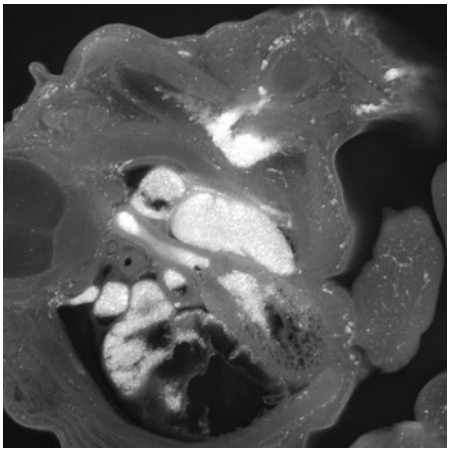

Figure 3. A raw fluorescence microscopy image from EFIC along the XY plane. The bright region is the fluorescence from blood within the embryonic heart. It is apparent that the XY resolution is significantly higher than the YZ (fig 4).

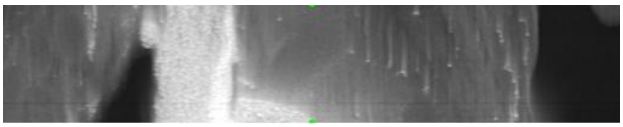

Figure 4. Image of a 3D dataset along the YZ plane (side view) where each horizontal line represents one z-plane. The direction of successive cutting and image acquisition is from the top to the bottom of this image

Before we design a restoration filter, the PSF of the imaging system needs to be determined.

A theoretical spatial frequency amplitude transfer function for 3D objects can be modelled by a *sinc* function [10], as

$$I(\omega_x,\omega_y,\omega_z)=\left(\frac{\sin(\omega_x/4)}{\omega_x/4}\cdot\frac{\sin(\omega_y/4)}{\omega_y/4}\cdot\frac{\sin(\omega_z/4)}{\omega_z/4}\right)^2 \qquad (1)$$

In this paper, we focus on the problem of correction of the episcopic fluorescence microscopy images along the z direction. In the XY plane the size of the PSF can be assumed to be very small compared to the size along the Z direction, therefore ω_x and ω_y can be assumed as an infinite signal in the frequency domain, namely a δ function. Thus, equation 1 can be simplified into equation 2 and the optimization is reduced into a one parameter optimization.

$$I(0,0,\omega)=I(\omega)=\left(\frac{\sin(\omega/4)}{\omega/4}\right)^2 \qquad (2)$$

In the frequency domain, the error function can be expressed as

$$Error(\omega)=Arg_\omega\left\|I(\omega)-\left|\iiint p(x,y,z)e^{-i(ux+vy+wz)}dxdydz\right\|\right\|_2^2 \qquad (3)$$

where p(x,y,z) is the psf approximation extracted from the raw data. The function (Error(ω)) should be

ISSN: 1727-1983

minimised with respect to the optical transfer function $I(\omega)$. Figure 5 presents the flow diagram for the restoration of episcopic fluoresence microscopy images which is roughly divided in two steps, a) PSF determination and b) deconvolution. There are three steps to generate a theoretical PSF. The first step is the fourier transform of an isolated raw data image P(x,y,z) which is selected from the experimental image stack and contains a psf-like point (fig 11). The second step is application of GDA to obtain the optimum (ω) in the sinc function which minimises equation 3. The third step is the inverse fourier transform of the *sinc* function to get the theoretical PSF in the spatial domain.

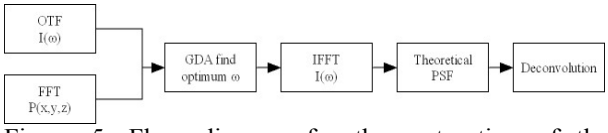

Figure 5. Flow diagram for the restoration of the episcopic fluoresence microscopy images.

Although GDA needs more iterations than other optimisation algorithms, such as the conjugate gradient algorithm (CGA), it converges to the global minimum values in most cases. The raw data is fitted by minimising the summed square error between the target and original functions, $E = \sum [p[n] - \hat{y}(n)]^2$, and raw data. Gearhart [11] expanded sinc(ωx) as

$$sinc(\omega x) = \sum_{n=0}^{N} (-1)^n \frac{(\omega x)^{2n}}{(2n+1)!} \tag{4}$$

Equation 4 can be expanded into a matrix expression

$$sinc(\omega x) = \begin{bmatrix} 1 & \cdots & \cdots & 0 \\ 0 & x_1^2 & \cdots & 0 \\ \vdots & \ddots & \ddots & 0 \\ 0 & \cdots & \cdots & x_{n-1}^{2n} \end{bmatrix} \cdot \begin{bmatrix} 1 \\ -\frac{\omega_1^2}{3!} \\ \vdots \\ -\frac{(-1)^{n-1}\omega_{n-1}^2}{(2n-1)!} \end{bmatrix} \tag{5}$$

then we have

$$\hat{y}(\omega) = sinc(\omega x) = X\omega \tag{6}$$

Replacement of $\hat{y} = X\omega$, **ω** is a weight matrix or vector and has parameters in the target function. Therefore, it has only one unique extremum where the first derivative of **E** with respect to **ω** is zero, assuming that $X^T X$ is not zero.

$$\frac{\partial E}{\partial \omega} = 2X^T X\omega - 2X^T p = 0 \tag{7}$$

$\omega = (XX^T)^{-1} X^T p$ is not quadratic and hence the normal inverse does not exist. For this reason GDA is used to find the optimum solution and calculate the inverse matrix. The GDA is described below where α is an iterative step and ε is a tolerance. The algorithm is based on adapting parameters in the direction of the negative gradient of E.

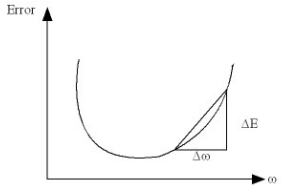

Figure 6. The error is minimised when the slope of gradient is zero.

$$\Delta\omega = -\alpha \frac{dE}{d\omega} \tag{8}$$

$$\Delta E = \Delta\omega \cdot \frac{dE}{d\omega} \tag{9}$$

where α>0 is small enough to ensure $\delta E \approx \Delta E$ Substituting (8) into (9) gives

$$\delta E \approx -\alpha \left(\frac{dE}{d\omega}\right)^2 \tag{10}$$

The −α term in equation 10 ensures that δE < 0. Then we can travel down the curve towards the minimum point as required (Figure 6). If we keep repeating these steps, we should approach the value ω* associated with the function minimum. The implementation of the GDA is summarised as:

1 Initialise $\omega=\omega_0$;
2 Test $\omega 1=\omega_0+\Delta\omega$ In the first iteration set $\Delta\omega=1$;
3 If $dE/d\omega>0$ then $\omega_1=-\omega_1$; if - $dE/d\omega>0$ then descrease $\Delta\omega$ and repeat 2
4 $\omega_{i+1}=\omega_i+\alpha\, dE/d\omega_i$
5 If $E_{i+1}>E_i$ or $dE/d(\omega_{i+1})<\varepsilon$ then stop and go to end;
If $E_{i+1}>E_i$ and $dE/d(\omega_{i+1})>\varepsilon$; change α and repeat from 3
6 End;

This algorithm always converges to the minimum correctly, independently of whether the initial value (ω_0) and next point (ω_1) are on the same side or on either side of the minimum as shown in Figure (7a) or (7b) respectively. A reversed value $-\omega_1$ is used if the search direction is along the ascent slope. The reversed direction is the descent slope of $\partial E/\partial\omega$, see Fig. (7a). However, if the reversed ω_1 is still along the ascent direction, (Fig. 7b), the minimum must be between ω1 and $-\omega_1$. After the reversion of $-\omega_1+\Delta\omega$, the minimum point can be approached from another side of the slope. The minimum point is found when either the gradient falls below tolerance (ε) or when any other point has a higher error, as would be the case at the minimum point.

There are many deconvolution algorithms successfully employed to restore blurred 2D and 3D microscopy images. Among those are the Wiener Filter,

ISSN: 1727-1983

the nonlinear Maximum Likelihood Estimate and Zhu's Penalty Likelihood restoration of 3D confocal images [12]. Unfortunately, none of these can be used with asymmetrical PSFs because in the frequency domain, the OTF is not phase free and 'ghosts' will be introduced into the restored images. Therefore, in this paper we employed the Landweber deconvolution algorithm (LWA) which is an efficient algorithm to be used with asymmetrical PSFs. The detailed description of LWA can be found elsewhere [13-15].

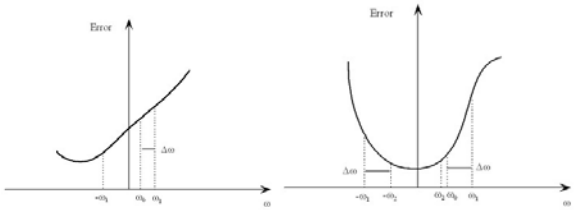

(a) Searching in one side (b) Searching in both sides

Figure 7. Initial values for gradient descent algorithm

Material and Methods

The data images were collected with a Leica episcopic fluorescence microscope. The sample was the heart from a stage E14.5 mouse embryo tagged with green fluorescent protein (GFP). The excitation and emission wavelengths were 480-510nm and 520nm respectively (Leica GFPPlus filter set). The objective on the stereo microscope was a 1x Plan Apo lens which gives a field of view of 10mm×10mm in the XY plane. The size of the digital image was 700×700 pixels, therefore each pixel represents 14.2µm. The exposure time for each image was 1.5s. After each image was taken, a slice 2 µm thick was removed from the top of the wax cube. The total number of slices along the z direction was 100 and therefore the thickness of the cube was 200µm along the z-axis, with each pixel representing a thickness of 2 µm.

Results and Discussion

Reconstructing the 3D data, we notice that there are several bright points whose signal is visible through the tissue for 10-20 microns above their exact location (Fig 4). From the side view this is seen as a spot with smeared tail. The smeared tail is the unwanted fluorescent light originating from tissue beneath the surface of the specimen. It is however an ideal estimate of the system PSF. Therefore, an isolated tailed point is selected from the virtual YZ image as a raw PSF.

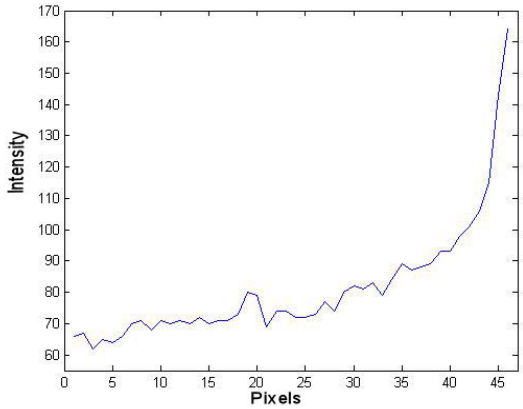

(a) 1D plot along the original tailed point in spatial domain

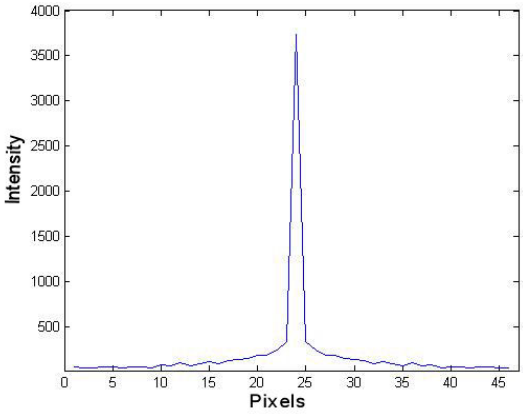

(b) Magnitude part in the Fourier domain

Figure 8. The original 1D signal in the spatial and frequency domains

Figure 8 shows a 1D graph of the original PSF data in the spatial and frequency domains. Figure 9 presents the original signal in the frequency domain and the modelled sinc function with an optimum ω (Fig.9b). Figure 10 shows the minimisation of log(error) with respect to ω. Figure 11 presents the original isolated point and the optimized sinc functions in the spatial domain. The modelled sinc function with the optimum ω will be used for the deconvolution of the 3D microscopy images.

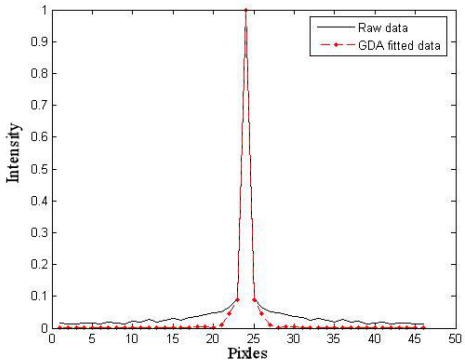

Figure 9. GDA modelled Sinc function

ISSN: 1727-1983

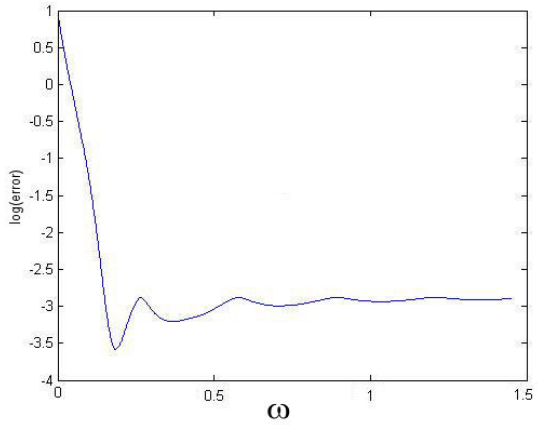

Figure 10. Plot of the error as it is minimised with respect to ω

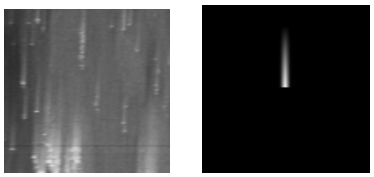

Figure 11. Original isolated point vs. theoretical PSF

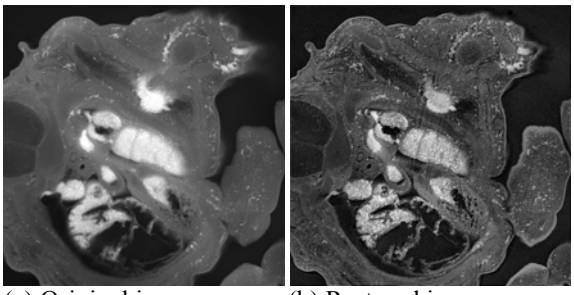

(a) Original image (b) Restored image

Figure 12. The 33rd slice from the original dataset and the LWA restored images using the GDA modelled PSF

Figure 12 shows one of the original fluorescence microscopy images and its restored equivalent using LWA with the *sinc(ω)* modelled PSF. It is obvious that the restored image has better resolution and sharper edges than the original. As a consequence, the restored image is more valuable for 3D visualization and analysis.

Conclusions and Future Work

The PSF measurement or modelling of an imaging system is an important prerequisite to the design of an efficient restoration filter for the restoration of the degraded 3D microscopy images. In this paper, we analysed the degradation model of the episcopic fluorescence imaging system. We classified the degradation into a diffusive motion-like blur along the z-axis. However there were no previously published data on PSF modelling for such blur. In this work, we employed an optimization algorithm (GDA) and used a target function (sinc) to find the optimum parameter (ω) which is used to control the bandwidth of OTF in the frequency domain. The inverse fourier transform of the modelled sinc function provides the PSF of the EFIC in the spatial domain. The modelled PSF was then combined with the Landweber deconvolution algorithm to restore the 3D episcopic fluorescence microscopy images. The optimum parameter (ω) for the sinc function was determined by finding the minimum error between the raw data and the target function using the GDA. The experimental results prove that GDA is indeed a reliable algorithm to find a global minimum value.

In this work, we used one isolated spot in order to approximate the PSF from the orignal raw data. Future work will focus on finding the relationship of the parameter (ω) in the sinc function to the experimental parameters of the imaging system, such as the image resolution, objective lens, thickness of the slice, emission wavelength and exposured time. Based on these experimental parameters, the system should automatically generate a reasonable PSF, bypassing the need to find isolated spot-like features in the raw data.

References

[1] WENINGER W.J. and MOHUN T., (2002): 'Phenotyping transgenic embryos: A rapid 3D-screening method based on Episcopic Fluorescence Image Capturing (EFIC)', *Nature Gen*, **30:59**-65

[2] ZHU D., RAZAZ M., HEMMNINGS A. and WANG B., (2004): 'Multiple point spread function modelling for deconvolution of 3D X-Ray diffraction data', *Journal of X-Ray Science and Technique*, 12**:179**-194

[3] RAZAZ M., LEE R.A., BELTON P.S. and WRIGHT K.M., (1998): 'A new approach for restoration of NMR signal', *Signal Processing IX, Theories and Application*, **2:841-844**

[4] RAZAZ M., LEE R.A., BELTON P.S. and WRIGHT K.M., (2000): 'A new algorithm for deconvolution of NMR spectra and images', *Image Processing, Mathematical Method and Application*, 2**:94-114**

[5] QUABIS S., DORN R., EBERLER M., GLOCKL Q. AND LEUCHS G., (2001), 'The focus of light-theoretical calculation and experimental tomographic reconstruction', *Applied physics B Lasers and Optics*, B72:109-113

[6] PRATT K.,(2001) 'Digital image processing', (John Wiley and Son, New York), (3rd Ed)

[7] Dekker den A.J.,(1997) 'Model-based optical resolution', IEEE Transactions on instrumentation and measurement, 46:798–802

[8] Zhu D., (2004) 'Reconstruction of X-Ray Diffraction and Confocal Images Using Iterative Deconvolution Techniques' PhD thesis, University of East Anglia,

[9] Razaz M. and Lee R. (1997), 'Comparison of an iterative deconvoltion and Wiener Filter for image

ISSN: 1727-1983

restoration', Image Processing Mathematics and Application, (Oxford University Press), p. 145-159

[10] van der Voort, H. (1989), '3D Image Formation in Hight-aperture Fluorescence Confocal Microscopy: a Numerical Analysis', Journal of Microscopy, 153, pp. 123-132

[11] Gearhart W.B. and Shultz H.S. (1990), 'The Function sinx/x', The Collage Mathematics Journal, 21:90-99

[12] Zhu D. and Razaz M. (2005): 'Adaptive penalty likelihood for reconstruction of multidimensional confocal microscopy images', Computerized Medical Imaging and Graphics, 29:319–331

[13] Bertero M. and Boccacci P. (1998): 'Introduction to Inverse Problems in Imaging', (Institute of Physics Publishing)

[14] Zhu D., Razaz M. and Lee R. (2004), 'A Landweber Algorithm for 3D Confocal Microscopy Restoration', Proc. of 17th International Conf. on Pattern Recognition, Cambridge of University, p.302-306

[15] Civanlar M. and Trussell H. (1985), The Landweber iteration projection onto convex set, IEEE Transactions on AcousticsSpeech and Signal Processing, ASSP-33:1632–1634

ISSN: 1727-1983